Shocks in the Evolution of an Eroding Channel

Edward Welsh[a], Björn Birnir[b,c,*] and Andrea Bertozzi[d]

[a] *Department of Mathematics, Westfield State College, Westfield, MA 01086, USA*

[b] *Department of Mathematics, University of California at Santa Barbara, CA 93106, USA*

[c] *University of Iceland, Science Institute, 3 Dunhaga, 107 Reykjavík, Iceland*

[d] *Department of Mathematics, University of California at Los Angeles, CA 90095, USA*

October 16, 2006

Abstract

Analysis of an evolution model for a river channel shows how three types of shocks determine the profile of the channel. This model shows that in a young river channel, evolution is driven by a small perturbation magnifying into a bore followed by a hydraulic jump. This mechanism produces a convex profile typical of young landscapes. A small knickpoint then develops at the bottom of the unstable convex profile. This knickpoint evolves into a diffusive shock which travels upslope, digging into the convex profile until the profile becomes concave, typical of mature landscapes.

1 Introduction

The evolution of a one-dimensional river channel on an eroding landscape is a challenging problem with many potential applications. Firstly, one would like to understand the general topography of a river profile as the river digs itself into an eroding landscape that may be eroding at a slower rate than the riverbed. Secondly, the evolution of such a one-dimensional profile gives information about the evolution of the entire two-dimensional landscape, since both water and sediment flow along gradient paths: these one-dimensional gradient paths to some extent shape the whole surface. Thirdly, landscape evolution is a very unstable and noisy process. The instabilities magnify the (white) noise that is always present in nature and give it a characteristic coloring. One dimensional channels allow us to study the details of this coloring process. The end result is large noise that is characteristic of the system and drives its evolution.

The paper that laid the foundation for all subsequent work in landscape evolution was written by Smith and Bretherton in 1972 [19] and many subsequent papers [15, 5, 2, 6] are essentially attempts to make small modification of the Smith and Bretherton

*Corresponding author. *E-mail address:* birnir@math.ucsb.edu

(SB) model. The problem that Smith and Bretherton ran into was that all reasonable hillslopes were unstable in their model. This instability was similar to the backward heat equation, where the modes associated with the highest frequencies grow the fastest and this precluded any numerical analysis of the nonlinear SB model.

However, in the mid nineties the advance of modern computers, in particular parallel computers towards the end of the century, made it possible to solve the SB model numerically with the instabilities present. It was found that the nonlinear term in the equations saturated the growth of the instabilities and it was possible to evolve reasonable landscapes numerically, using physically based models. These results were published in two papers by Smith, Birnir and Merchant [20, 18].

It quickly became clear with the appearance of the new numerical results that noise plays a large role in the evolution of the solutions of the SB model. This may be surprising, because the SB model is deterministic, but the explanation is the effect of the instabilities on the noise that is always present in the environment–in particular on any realistic landscapes. The white noise is magnified by the instabilities and saturated by the nonlinearities into large colored noise that drives the equations. Thus effectively the numerical solution of the SB model is a stochastic process, solving a nonlinear stochastic partial differential equation driven by large colored noise. This stochastic process can be characterized by the scaling properties of its associated statistical quantities (the variogram) and this was done by Birnir et al. [4]. The numerical methods are very sensitive to the magnification of the noise by the instabilities. It was shown in the thesis of G. Merchant [11] that whereas implicit numerical methods produce correct scaling of statistical quantities, explicit methods do not. However, the latter capture the large-scale features of the evolving surface. More recently the stochastic processes determining the evolution of the landscapes have been found and proven that they do have the correct scaling properties: see Birnir et al. [3].

In a 2000 paper Smith et al. [16] found all one-dimensional stationary solutions and classified them. These can be thought of as particular geographic formations where perturbations in the transverse direction are suppressed. More usefully these solutions are the profiles of river channels that have already formed and are evolving. Smith and his collaborators did not connect the various profiles by a dynamic evolution but that was done in the thesis of E. Welsh [21] and is carried further in this paper. It will be shown that an initially linear profile will develop a shock in the water flow when a small perturbation is inserted at the top. This shock is a bore that propagates downstream; in the wake of the shock is another shock in the water surface: a hydraulic jump that digs up sediment. In the increased water volume between the stationary hydraulic jump and the traveling bore sediment is deposited. If this process is repeated in several storms it results in a convex hillslope. Once the convexity meets the lower boundary, a small concavity is created. This creates a shock in the gradient of the sediment flow; its profile in the riverbed is called a knick point. The shock travels upstream. Once it gets all the way to the top of the hillslope, it will have carved out a concave profile. This is the evolution of the transport limited river profile and proves the conjecture made by Birnir, Smith and Merchant in [4]. Bores and hydraulic jumps are widely observed and it is well known that knick points (rapids) travel upstream in time.

How rivers are formed is a harder problem and is still open. Partial results have been obtained recently Mertens, Putkaradze and Vorobieff [12], investigating the formation

of a river and its meandering on a non-erodable surface. In these experiments surface tension plays a role but one can show that for real channels surface tension is negligible. The existence of channels on the surface also plays a role in the formation of a river, but the general direction of the river is a random walk among the channels already existing on the surface. In this paper we have assumed that the river has already formed and study its evolution.

Note that the surface of interest–the water surface–is the water we imagine covers the land surface, at least during big rainstorms. Because water can concentrate on some parts of the land surface, the water surface can have gradients different from those of the land surface. Water surface gradients, not land surface gradients, drive both water and sediment flow, and it is for this reason that we focus on the water surface. We will see that the equations in the SB model are one-dimensional in the direction of this water surface gradient. Because of this, our analysis uses the modern theory of shock formation and propagation (see P. Lax [9]) to do both analysis and numerics and compare the two. This analysis in one spatial dimensional therefore has some applicability to a two-dimensional water surface.

In the sections to follow, we will describe the SB model and adapt it for use along a river channel. We will then provide a careful analysis of the magnification of a small perturbation as it forms a shock, or bore, in the water depth in the special case of water surface fixed in time. We then show how the full SB model also magnifies a small perturbation, creating a bore in both water depth and water surface, followed by a hydraulic jump. These mechanisms create a young, convex hillslope after repeated application. Because this hillslope is unstable, the SB model forms a knickpoint at the lower reaches of the slope. This knickpoint is emblematic of a "colored" process, and as it proceeds upslope, it creates a mature, concave profile. These processes tell the whole story of the evolution of the river profile after the river channel itself has formed.

2 The Model

As presented in [18], the SB model begins with continuous land surface elevation $z = z(x,y,t)$, water depth $h = h(x,y,t)$, and the free water surface $H = z + h$. If we assume water flux per unit width (q_w) and sediment flux per unit width (q_s) both flow downhill according to the free surface (that is, in the direction $-\frac{\nabla H}{|\nabla H|}$), then conservation of water mass and conservation of landmass give us the coupled pair of partial differential equations

$$\frac{\partial h}{\partial t} = R + \nabla \cdot \left(\frac{\nabla H}{|\nabla H|} q_w \right) \tag{1}$$

$$\frac{\partial z}{\partial t} = U + \nabla \cdot \left(\frac{\nabla H}{|\nabla H|} q_s \right) \tag{2}$$

where R is the rainfall rate, and U is the rate, generally uniform in both space and time, at which the land surface is lifted by geologic forces from below ("tectonic uplift" or "uplift"). Because rainfall and tectonic uplift operate on very different timescales, we examine our model on two timescales. (See [4] for a thorough discussion of scales.)

The initial land surface z will be approximately an inclined plane, sloping primarily in the x direction, on which a river channel has already formed. No water or sediment will flow in at the top edge of the domain ($x = 0$), which we consider to be a ridgeline. An absorbing body of water at the bottom of the slope ($x = x_{\max}$) will carry away all water and sediment there. We will use periodic boundary conditions in the transverse (y) direction (corresponding to an unending ridge).

Because both water and sediment flow in the direction of the unit vector $\frac{\nabla H}{|\nabla H|}$, we will reduce our equations to a single spatial dimension, as in the analysis in Appendix A of [4]. In one spatial dimension, let H slope down from its maximum at $x = 0$ to height h_b at $x = x_{\max}$. In this case, $|\nabla H| = |H_x| = -H_x$ over the entire domain (as long as the water surface slopes down from left to right). Because most of the erosion occurs during big storms (that is, under turbulent conditions), we will use turbulent flow velocity $v = h^{2/3}|\nabla H|^{1/2}$, giving us water flux $q_w = h^{5/3}|\nabla H|^{1/2}$. (Note that the water depth equation is a model for the average of the flow over many large rainstorms–see also [7, 13]–but the results are the same as for shallow water equations [17].)

Equation (1) becomes

$$\frac{\partial h}{\partial t} = R - \partial_x \left[h^{5/3} |H_x|^{1/2} \right]. \tag{3}$$

If we assume we have transport-limited erosion, we will use sediment flux $q_s = h^{10/3}|\nabla H|^3$ (corresponding to [14]), so equation (2) becomes

$$\frac{\partial H}{\partial t} - \eta \frac{\partial h}{\partial t} = U - \partial_x \left[h^{10/3} |H_x|^3 \right]; \tag{4}$$

when we use a scaling such as in [4]. The parameter η is small.

These equations will evolve forward from time $t = 0$ on a spatial domain $0 \le x \le x_{\max}$. Initial conditions $h(x,0)$ and $H(x,0)$ will be given. Boundary conditions are zero water depth, water flux, and sediment flux ($h = h^{5/3}|\partial_x H|^{1/2} = h^{10/3}|\partial_x H|^3 = 0$) at the top of the ridgeline ($x = 0$). We also assume zero elevation and prescribed water depth and water surface ($h = H = h_b$) at the bottom of the domain ($x = x_{\max}$).

Using the scaling arguments discussed in [4], we may evolve equation (3) on a short timescale on which $\frac{\partial H}{\partial t}$ is small. If we then evolve equation (4) on an intermediate timescale, we may eliminate the $\frac{\partial h}{\partial t}$ term from equation (4), obtaining

$$\frac{\partial H}{\partial t} = U - \partial_x \left[h^{10/3} |H_x|^3 \right]. \tag{5}$$

We may couple equations (3) and (5); it is also possible to use water depth steady-state information

$$0 = R - \partial_x \left[h^{5/3} |\partial_x H|^{1/2} \right] \tag{6}$$

in equation (5) and evolve the resulting single equation. Both schemes are useful.

We solve the water depth equation (3) following the classical theory of scalar conservation laws. Continuous solutions can be found using the method of characteristics [9] as we show below. Characteristics are the lines along which initial data is carried. In

addition, we consider solutions with shocks, which are jump discontinuities in the water thickness, occuring at a particular spatial position $X_s(t)$. The shock position moves with speed σ satisfying the Rankine-Hugoniot jump condition. For a conservation law of the form $h_t + (F(h))_x = 0$, the condition is that the jump in F divided by the jump in h must equal the shock speed. We view equation (3) as having this form, with the addition of a source term, R, the rainfall amount. The presence of the source term does not affect the Rankine-Hugoniot condition [9].

Below we present a special solution that is comprised of both a rarefaction fan (which we find using the method of characteristics) and a shock, satisfying the Rankine-Hugoniot condition. Such rarefaction-shock solutions occur in other shallow water models for liquid flow on surfaces (see e.g. the solution of Huppert for viscous flow down an incline [8] and more recent rarefaction-shocks in thermally driven films [1]).

We will examine three types of shocks that develop in this system. The first shock occurs in the water depth h when a large volume of water is suddenly introduced, for example by heavy rainfall. This behavior physically corresponds to a flood pulse or a bore in a riverbed. The second type occurs as a dramatic change in the water surface H behind the bore caused by a drop in water velocity and corresponds to a hydraulic jump. The third type of shock occurs when a young, unstable convex water surface develops a small concavity or "knickpoint." This type of shock physically corresponds to rapids. See the numerical illustration in Figures 13 and 14.

3 Bore Formation in the Water Depth

We now use characteristic analysis to describe when shocks will form in the water depth h. We will then find two solutions to the water depth equation (3), one very special and one more generic, using a fixed, constant-slope water surface H. This condition need not apply to the general characteristic analysis below.

Recall the water depth equation (3):

$$\begin{aligned} \frac{\partial h}{\partial t} &= R - \partial_x \left[h^{5/3} |H_x|^{1/2} \right]. \\ &= R - \frac{5}{3} h^{2/3} |H_x|^{1/2} h_x + \frac{h^{5/3}}{2|H_x|^{1/2}} H_{xx}. \end{aligned}$$

Let us examine how water depth h evolves along currents X with speed $\frac{5}{3} h^{2/3} |H_x|^{1/2}$. We can formally define these trajectories, or characteristics, by

$$X(s,0) = s \tag{7}$$

and

$$\left. \frac{dX}{dt} \right|_{(X(s,t),t)} = \left. \frac{5}{3} h^{2/3} |H_x|^{1/2} \right|_{(X(s,t),t)}, \tag{8}$$

equation (3) may be represented in Lagrangian form as

$$\frac{d}{dt}h = R + \left.\frac{h^{5/3}}{2|H_x|^{1/2}}H_{xx}\right|_{(X(s,t),t)}, \tag{9}$$

which integrates to give the solution

$$h(X(s,t),t) = h(s,0) + Rt + \int_0^t \left.\frac{h^{5/3}}{2|H_x|^{1/2}}H_{xx}\right|_{(X(s,\tau),\tau)} d\tau. \tag{10}$$

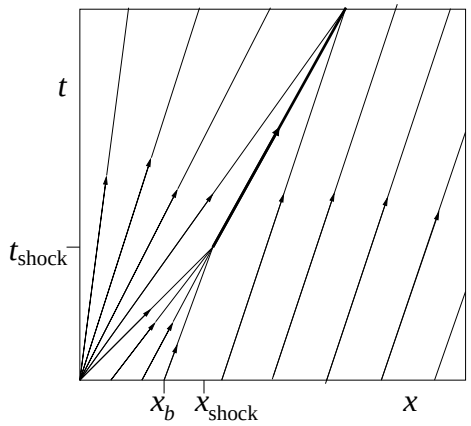

Figure 1: An example of characteristics (or trajectories) for water flowing down a constant slope. At time t_{shock}, characteristics originating between $x = 0$ and x_b intersect and form a **shock** (depicted in **bold**). Note the rarefaction fan to the left of the shock. The shock proceeds downslope; characteristics continue to enter the shock from both the left and the right.

Along a characteristic, or trajectory, water depth evolves according to equation (9); see several characteristics graphed in Figure 1. If rainfall R and water surface curvature H_{xx} are zero (or very small), equation (10) tells us that along characteristics, the water depth h is equal to (or very close to) the initial water depth. Whenever two or more characteristics intersect, as at time t_{shock} in the fi gure, a shock may form. Because these trajectories always travel to the right, any shocks that form will travel downslope.

3.1 A Special Solution for the Water Depth Equation

In the demonstrations to follow, k, $h_M > h_b$, and x_b are all positive constants, and rainfall R is 0. A more thorough treatment of the computations can be found on pp. 62-70 of [21].

Recall that we are using a fi xed, constant-slope water surface $H(x) = k^2(x_{\max} - x) + h_b$. We will examine the conveniently chosen initial water depth h:

$$h(x,0) = \begin{cases} 0 & x = 0 \\ \left(h_M^{2/3} - \dfrac{h_M^{2/3} - h_b^{2/3}}{x_b} x\right)^{3/2} & 0 < x \leq x_b \\ h_b & x_b < x \leq x_{\max} \end{cases} \tag{11}$$

Because the characteristics resolve very nicely for this particular initial condition, we can find an exact solution $h(x,t)$. Solving the characteristic equation (8), we find that, in the absence of a shock,

$$s = \frac{x_b(X(s,t) - \frac{5}{3}kh_M^{2/3}t)}{x_b - \frac{5}{3}k(h_M^{2/3} - h_b^{2/3})t} = \frac{x_b(X(s,t) - v_M t)}{x_b - (v_M - v_b)t} \tag{12}$$

with the constant velocities $v_M = \frac{5}{3}kh_M^{2/3}$ and $v_b = \frac{5}{3}kh_b^{2/3}$.

Note that several characteristics emanate from $s = 0$. Each value of h between 0 and h_M is carried on a characteristic with speed $\frac{5}{3}kh^{2/3}$; these different characteristics spread out, forming a rarefaction fan, appearing along the t-axis in Figure 1. In this rarefaction fan,

$$h(x,t) = \left(\frac{3x}{5kt}\right)^{3/2}. \tag{13}$$

Outside the rarefaction fan,

$$h(x,t) = \left(\frac{h_M^{2/3}x_b - x(h_M^{2/3} - h_b^{2/3})}{x_b - (v_M - v_b)t}\right)^{3/2} \tag{14}$$

since water depth h is preserved along characteristics.

These formulas hold until a shock forms. At time

$$t_{\text{shock}} = \frac{x_b}{v_M - v_b} \tag{15}$$

(shown in Figure 1) all characteristics originating from the region $0 < s \leq x_b$ intersect at a single point

$$x_{\text{shock}} = \frac{h_M^{2/3}x_b}{h_M^{2/3} - h_b^{2/3}} \tag{16}$$

(shown in Figure 1) and the entire shock forms at this point.

After the shock forms, it travels on a special characteristic $X_s(t)$ according to the condition

$$X_s(t_{\text{shock}}) = x_{\text{shock}} \tag{17}$$

and the Rankine-Hugoniot condition

$$\frac{dX_s}{dt} = \sigma = \frac{\left(\frac{3X_s}{5kt}\right)^{5/3} k - v_b}{\frac{3X_s}{5kt} - h_b}. \tag{18}$$

This special characteristic is the bold curve in Figure 1. Note that a (messy) closed-form equation relating X_s and t exists, but it cannot be explicitly solved for X_s. Characteristics continue to enter the shock from both sides, so this shock is physical.

Collecting all of the information, we have

$$h(x,t) = \begin{cases} \left(\frac{3x}{5kt}\right)^{3/2} & x < v_M t \text{ and } x < X_s(t) \\ \left(\frac{h_M^{2/3} x_b - x(h_M^{2/3} - h_b^{2/3})}{x_b - (v_M - v_b)t}\right)^{3/2} & v_M t \le x < v_b t + x_b \\ h_b & v_b t + x_b \le x \le x_{\max} \text{ and } x > X_s(t) \end{cases} \tag{19}$$

where $X_s(t)$ obeys equations (17) and (18). We can see the three portions of this solution in Figure 1: the first portion is the rarefaction on the left of the graph, the second is the small triangle with base $0 \le x \le 0.2$, and the third is the collection of parallel characteristics on the right.

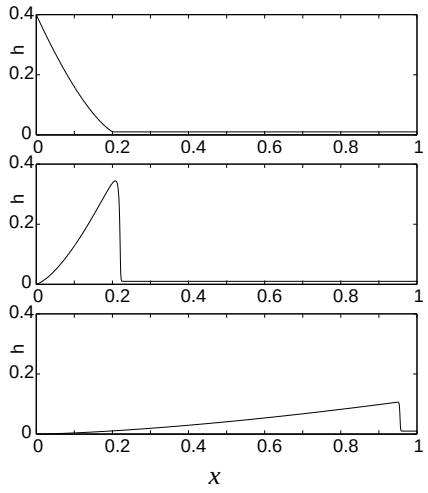

Figure 2: Water depth h at times $t = 0$ (top), $t = .54$ (center), and $t = 5.7$ (bottom). Note the rarefaction wave on the left. After the shock forms, it travels downslope and decreases in height.

The exact solution (19) is indistinguishable from an approximation generated by a numerical scheme. Set $k = \sqrt{.2}$, $h_M = 0.4$, $h_b = 0.01$, $x_b = 0.2$, and $x_{\max} = 1$. We use an upwind scheme, see LeVeque [10], subdividing the domain into 1000 cells of

size $\Delta x = .001$; a timestep of $\Delta t = .001$ is short enough to accommodate the fastest characteristic with speed $v_M = \frac{5}{3}h_M^{2/3}k \approx .4046$. See the results in Figure 2.

To further test the numerical scheme, we record the height and speed of the shock in the numerical solution at each time step. We can compare this height to the value predicted by characteristic information. We can also track the speed of the shock in the numerical solution and compare it to that predicted by the Rankine-Hugoniot condition (18). Observed shock height gives a second prediction of shock speed. Height and speed comparisons are graphed over time in Figure 3.

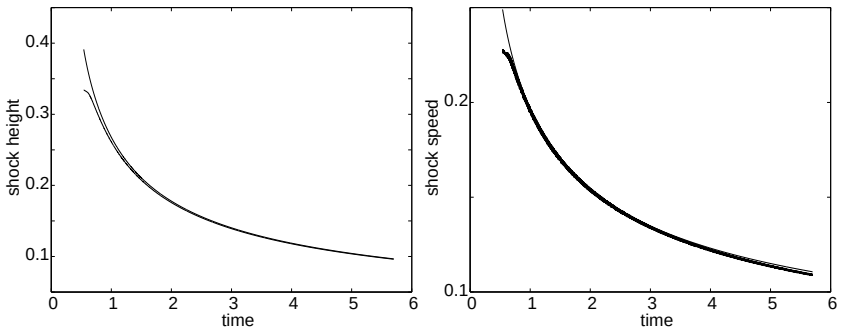

Figure 3: Shock height (left) and speed (right) over time. Note that the exact solution predicts a larger and faster shock initially; the prediction and numerics agree very closely after time $t = 1$.

The predicted values are very close to the observed values, demonstrating that the upwind scheme respects shock behavior. Shock formation is not specific to this one example. Let us use these numerical tools to examine a more generic perturbation of initial water depth.

3.2 Model for Magnification of a Small Perturbation

In nature, small bumps may appear uniformly distributed in the water thickness. (Think of raindrops.) To understand what happens to these bumps, we will examine a small, generic perturbation in water depth and see if it forms a shock under the SB model. Consider the small Gaussian initial condition

$$h(x,0) = \frac{1}{4}h_b \exp\left[-\left(\frac{x-0.1}{0.05}\right)^2\right] \tag{20}$$

For ease of analysis, we will again use the fixed H of constant slope $H(x) = k^2(x_{\max} - x) + h_b$. (We will relax this condition when we analyze the full system in the next section.) As before, k and h_b are positive constants, and rainfall R is 0.

It is not possible to do a complete characteristic analysis as with the previous example, but we can extract some useful information. The characteristic $X(0.1,t)$ carries $\frac{5}{4}$ as much water as the (essentially) base-level characteristic $X(0.2,t)$, so it will travel

about 16% faster, and overtake the slower characteristic at about $x = 0.8$. We expect a shock to form here.

Using an upwind scheme, we will model the evolution of the Gaussian initial water depth according to equation (3):

$$h_t = R - \partial_x \left[h^{5/3} |H_x|^{1/2} \right]$$

with $h(0,t) = 0$. We will again examine the formation of the shock and track its progress. The water surface H is still held fixed with constant slope: $|H_x|^{1/2} = k$, and rainfall R is zero. We use initial water depth (20). As before, $k = \sqrt{.2}$, $h_b = .01$, and $x_{\max} = 1$; the domain is subdivided into 1000 cells of size $\Delta x = .001$. A timestep of $\Delta t = .02$ is short enough to accommodate the fastest characteristic with speed $v = \frac{5}{3}\left(\frac{5}{4}h_b^{2/3}\right)k \approx 0.0401$. See the results in Figure 4.

Here we see the magnification of a Gaussian initial condition: the portion downslope of the water depth maximum ($s = 0.1$) sharpens into a shock near $x = 0.8$, while the upslope portion joins the rarefaction wave. So we see that even small perturbations form shocks, regardless of their initial shape.

4 The Effect of Water Depth Shocks on the Water Surface

For our initial analysis, we have held the water surface (H) fixed in time. If we allow the water surface to evolve, what effect does the water depth shock have on the water surface? What effect does the changing water surface have on the water shock? We will examine these questions numerically.

Recall the water surface equation (5):

$$H_t = U - \partial_x \left[h^{10/3} |H_x|^3 \right].$$

We use a constant slope initial water surface $H(x,0) = k^2(x_{\max} - x) + h_b$, and maintain zero sediment flux $h^{10/3}|H_x|^3 = 0$ for $x = 0$ and all time $t \geq 0$, and fix $H(x_{\max}, t) = h_b$. We will evolve equation (5) using an upwind scheme.

At the same time, we will use an upwind scheme to evolve the water depth equation (3):

$$h_t = R - \partial_x \left[h^{5/3} |H_x|^{1/2} \right]$$

with $h(0,t) = 0$ and the piecewise linear initial water depth (21):

$$h(x,0) = \begin{cases} 0 & x = 0 \\ h_M - \frac{h_M - h_b}{x_b} x & 0 < x \leq x_b \\ h_b & x_b < x \leq x_{\max} \end{cases} \tag{21}$$

As before, k, $h_M > h_b$, and x_b are all positive constants, and rainfall R is 0.

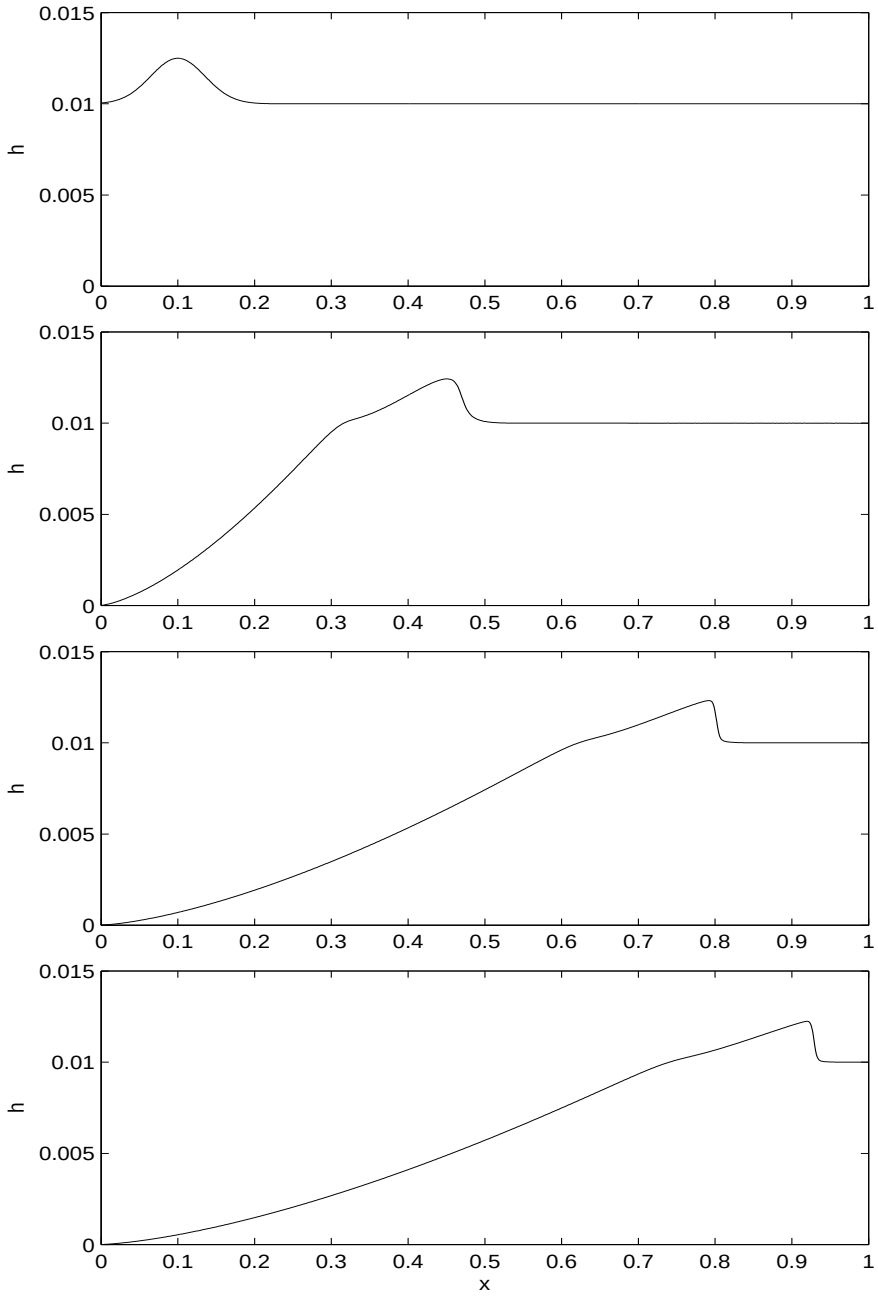

Figure 4: $h(x,0)$, $h(x,8.8)$, $h(x,17.6)$, and $h(x,21)$. The typical rarefaction wave forms, while the initial Gaussian magnifi es into a shock traveling downslope.

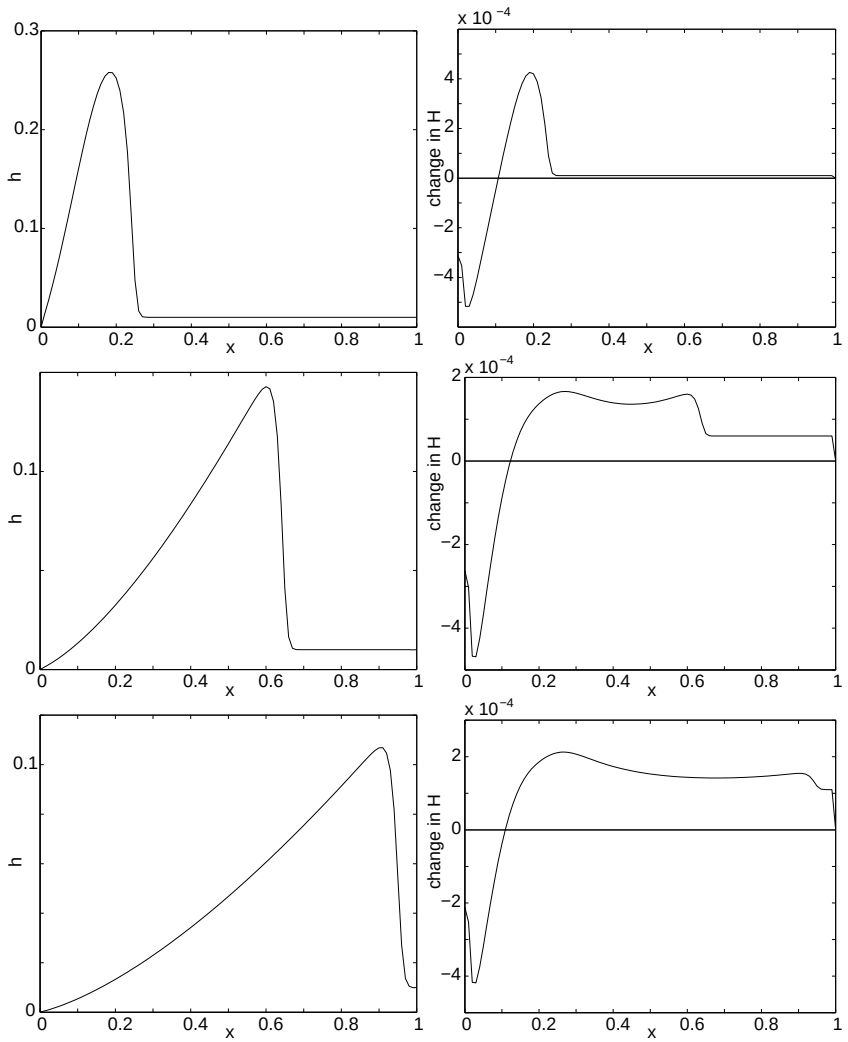

Figure 5: Water depth h (left) and change in water surface H (right) at times $t = .5$ (top), $t = 3$ (center), and $t = 5.5$ (bottom). The initial (zero) change in H is marked in the right-hand graphs. The hydraulic jump forms in the water surface at $x = 0.1$, and the water surface bore follows the water depth shock from $x = 0.2$ (top) to $x = 0.6$ (middle) to $x = 0.95$ (bottom).

Because the water surface equation (5) evolves on a timescale longer than the water depth equation (3), we may use a longer time step on equation (5). We evolve the water surface equation (5) two steps of size $\Delta t = .001$ for every ten steps of size $\Delta t = .005$ we evolve the water depth equation (3). We set uplift $U = .00002$, and the parameters $k = \sqrt{.2}$, $h_M = .4$, $h_b = .01$, $x_b = .2$, and $x_{\max} = 1$; the domain is subdivided into 100 cells of size $\Delta x = .01$; see the results in Figure 5. (An evaluation of the accuracy of this upwind scheme can be found in [21].)

Note that the coupled system produces a shock in the water depth, much as in the previous section. This shock is somewhat less sharp than before, because deposition at the shock front tends to smear it out.

The water surface H also forms a shock, or a bore, following the front of the water pulse down the hillslope. Upslope of the water pulse, another almost stationary shock–a hydraulic jump–forms as the rarefaction fan stretches out near the peak.

As the water pulse tracks down the surface, it loses some of its height and deposits sediment along the way. As time progresses, the effect of uplift becomes apparent on the lower reaches of the water surface. At time 5.5, the bore is about to exit the domain.

If we run this simulation to time $t = 25$, the water almost completely drains off the domain, as depicted in Figure 6. Note that there is a slight bulge of water above the level $h_b = .01$.

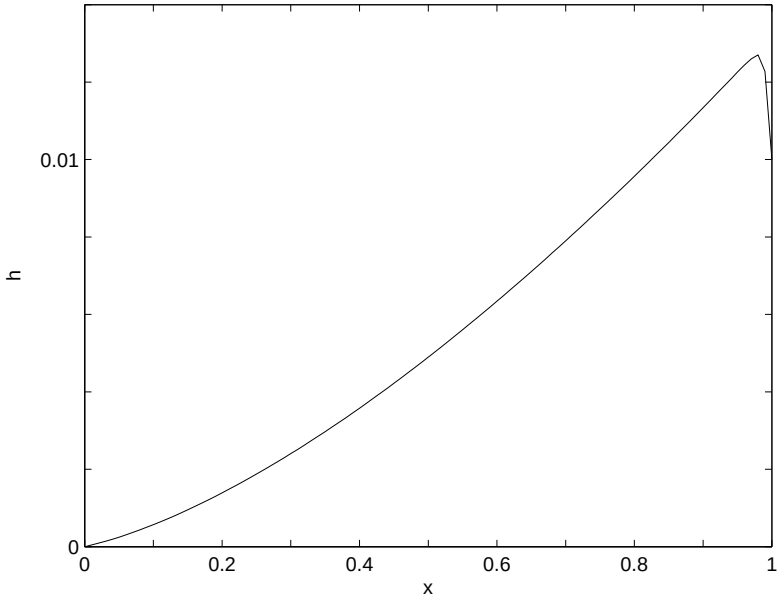

Figure 6: $h(x, 25)$

4.1 Repeated Shocks

The previous example models the progress of stormwater down a hillslope. What is the effect of repeated storms on this hillslope? At time $t = 25$, we re-initialize the water depth h and evolve the new system an additional 25 time units.

If we repeat this process, say, nine more times (for a total of ten storms), the water depth and change in water surface can be seen in Figure 7. The use of the subscript in h_{old} indicates that the next storm has not yet fallen.

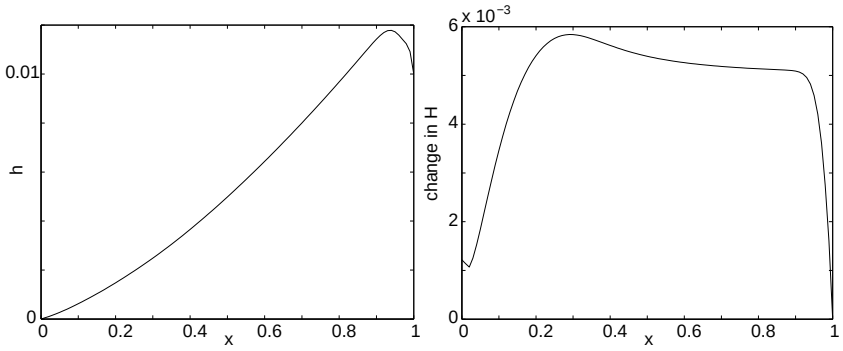

Figure 7: $h_{\text{old}}(x, 250)$ and $H(x, 250) - H(x, 0)$

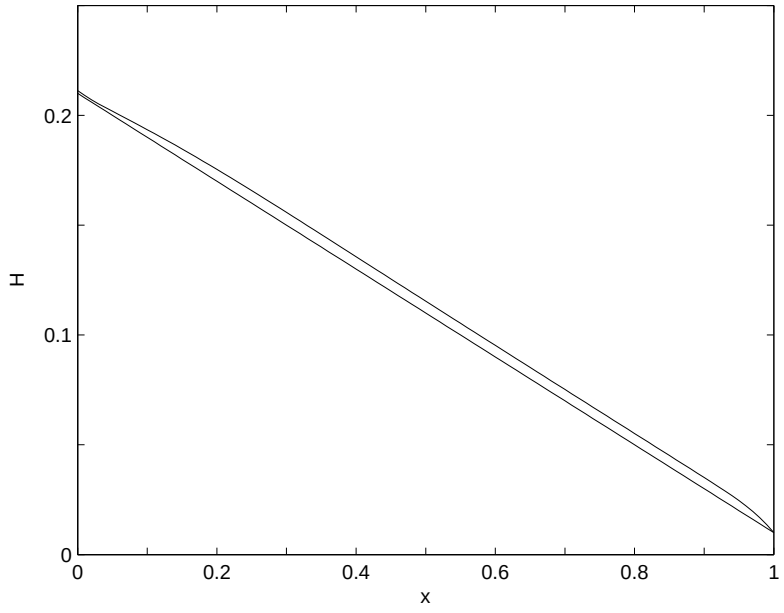

Figure 8: $H(x, 250)$ (curved) and $H(x, 0)$ (linear)

At this point, the accumulated effect of the storms on the water surface begins to become apparent; see Figure 8. The water surface is becoming visibly convex. The mechanism creating this convexity appears to be a combination of the hydraulic jump and the bore. Before the shock forms and as it forms, the water digs into the surface, leaving a hydraulic jump in the water surface. The hydraulic jump continues to dig up sediment and thus moves very slowly downstream. After the shock has fully formed, the bore redeposits this sediment. At the bottom of the slope, the bore has become smaller, and deposits less and less sediment. Combined with uplift and the lower boundary condition for H, we see a net gain in elevation through the middle of the do[illegible]

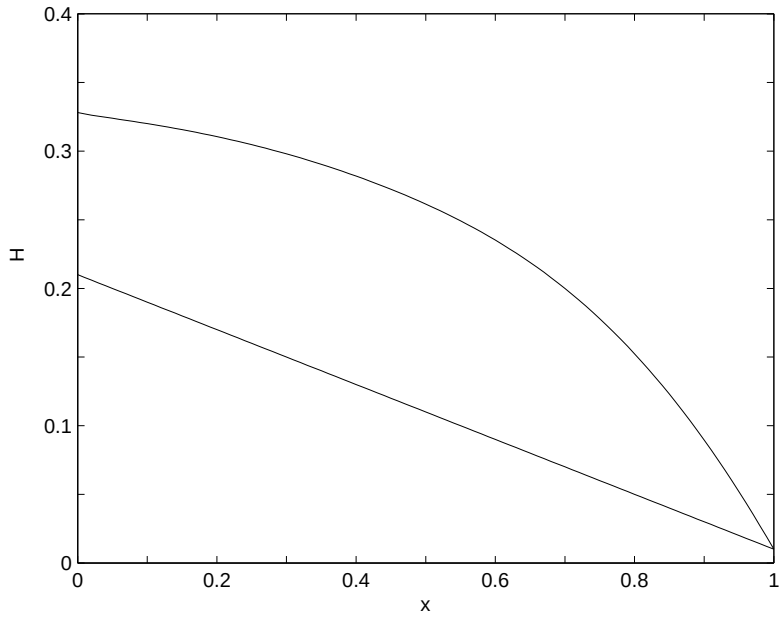

Figure 9: $H(x, 7500)$ (curved) and $H(x, 0)$ (linear)

After a total of 300 storms, the water surface has become quite convex. (See Figure 9.) Water will have drained quite completely at the end of this last storm. (See Figure 10.) The end of the domain is very steep, and thus able to clear the last traces of the storm more quickly than the initial slope could.

5 Shocks in the Water Surface Equation

If we resume a rainfall that is uniform in both space and time, the convex water surface profi les in the previous section become unstable. If uniform rainfall begins at time $t = 7500$, water depth moves quickly toward a steady-state in the waterflow with water concentrated at the bottom of the domain. Erosion is accelerated here, reversing the

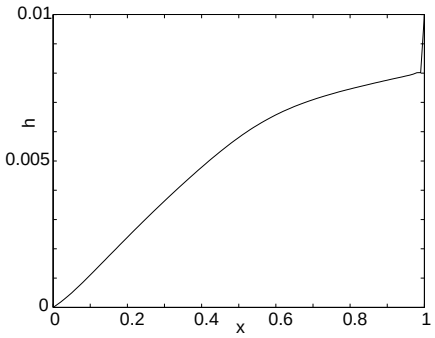

Figure 10: $h_{\text{old}}(x, 7500)$

curvature of the water surface, and forming a "knickpoint" or small concavity. As mentioned earlier, this knickpoint physically corresponds to rapids.

5.1 Creating the Water Surface Shock

Using the upwind schemes, we again evolve the water surface equation (5) two steps for every ten steps we evolve the water depth equation (3). Rainfall rate R is 0.02, and uplift U is 0.00002. We evolve equation (3) with a timestep of $\Delta t = .01$ and equation (5) with a timestep of $\Delta t = .05$.

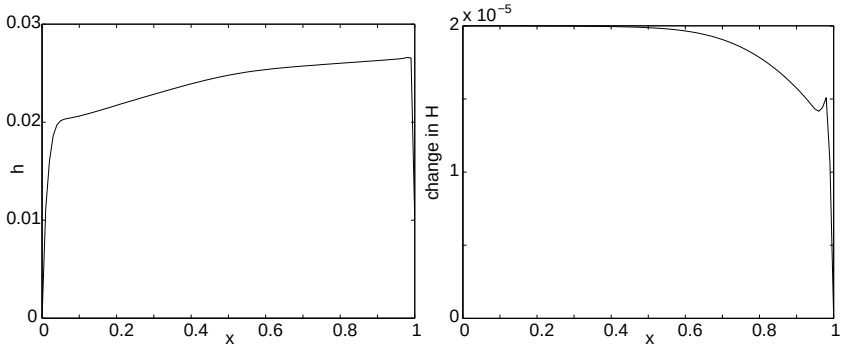

Figure 11: $h(x, 7501)$ and $H(x, 7501) - H(x, 7500)$

At time $t = 7501$, water becomes thicker at the lower end of the domain, and the knickpoint begins to become visible. See h and the difference $H(x, 7501) - H(x, 7500)$ in Figure 11. We see that the primary change in the surface is uplift, but the accumulating water on the lower end of the domain is beginning to dig a knickpoint.

If we continue to $t = 7510$, more water accumulates at the low end of the domain as the knickpoint in H becomes dramatically larger; see Figure 12. The change in H

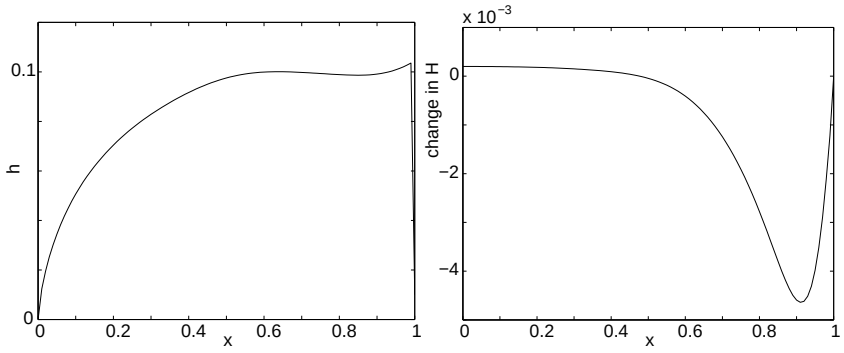

Figure 12: $h(x,7510)$ and $H(x,7510) - H(x,7500)$

can be seen (just barely) on the plot comparing $H(x,7500)$ and $H(x,7510)$ in Figure 13. $H(x,7510)$ is underneath $H(x,7500)$.

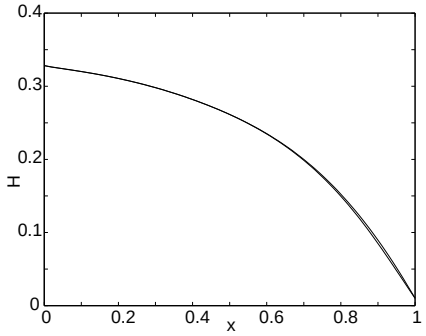

Figure 13: $H(x,7510)$ and $H(x,7500)$

By time $t = 7600$, the knickpoint is quite visible on the graph of H. It has formed and is traveling upslope; see Figure 14. It is also possible to see the change in concavity at the bottom of the domain. Note that water depth h is not changing greatly.

If we continue this evolution to time $t = 16\,000$, we see the entire water surface becoming concave, and singular at $x = 0$. In Figure 15, $t = 7500; 7600; 8500; 11000;$ and 16000. Notice that there is very little water towards the top of the ridge ($x = 0$).

5.2 Steady-States

In the short timescale, water depth h is in steady-state when $R = \partial_x \left[h^{5/3}|H_x|^{1/2}\right]$, or, integrating,

$$h_{ss}(x,t) = \frac{(Rx)^{3/5}}{|H_x|^{3/10}}. \tag{22}$$

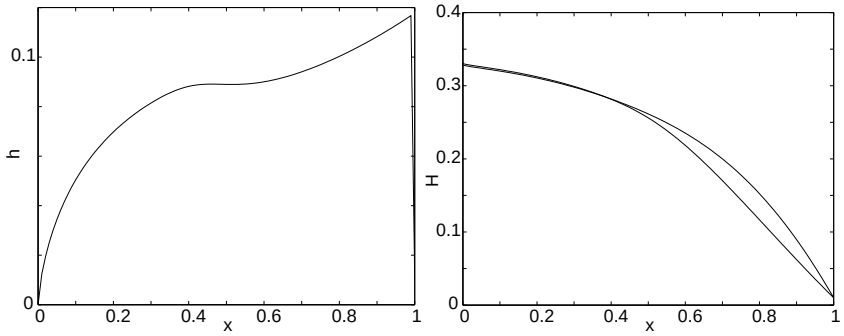

Figure 14: $h(x,7600)$; and $H(x,7600)$ with $H(x,7500)$

After time 7510, the transient h follows this steady-state very closely. Instead of evolving equation (3) on a faster timescale, we will use equation (22) to substitute for h in the water surface evolution equation (5), obtaining

$$H_t = U - \partial_x \left[R^2 x^2 |H_x|^2 \right]. \tag{23}$$

We will evolve this single equation past time 7510.

Note that this equation evolves to a steady-state of

$$H_{ss}(x) = h_b + \frac{2\sqrt{U}}{R} \left[\sqrt{x_{\max}} - \sqrt{x} \right] \tag{24}$$

around time $t = 16\,000$. This is precisely the steady-state predicted in [16].

5.3 Knickpoint: A Shock in the Water Surface

In transitioning to the steady, concave surface, it is worth investigating the potential for shock formation. If we use the substitution $S = |H_x| = -H_x$ and differentiate both sides of equation (23) with respect to x, we get

$$\begin{aligned} S_t &= R^2 \partial_{xx} \left[x^2 S^2 \right] \\ &= 2R^2 \left[x^2 S S_{xx} + x^2 S_x^2 + 4xSS_x + S^2 \right], \end{aligned} \tag{25}$$

a form suggesting characteristics $X(s,t)$ obeying

$$\frac{dX}{dt} = -2R^2 (x^2 S_x + 4xS). \tag{26}$$

Note the S_{xx} term in equation (25). Because this term has positive sign (unless $x = 0$), it will act like positive heat smoothing. Any shock in S will be diffusive.

If we track $S(x,t)$ at various times, we see a shock-like jump traveling across the domain from right to left. After running the fully transient scheme to time 7510, we

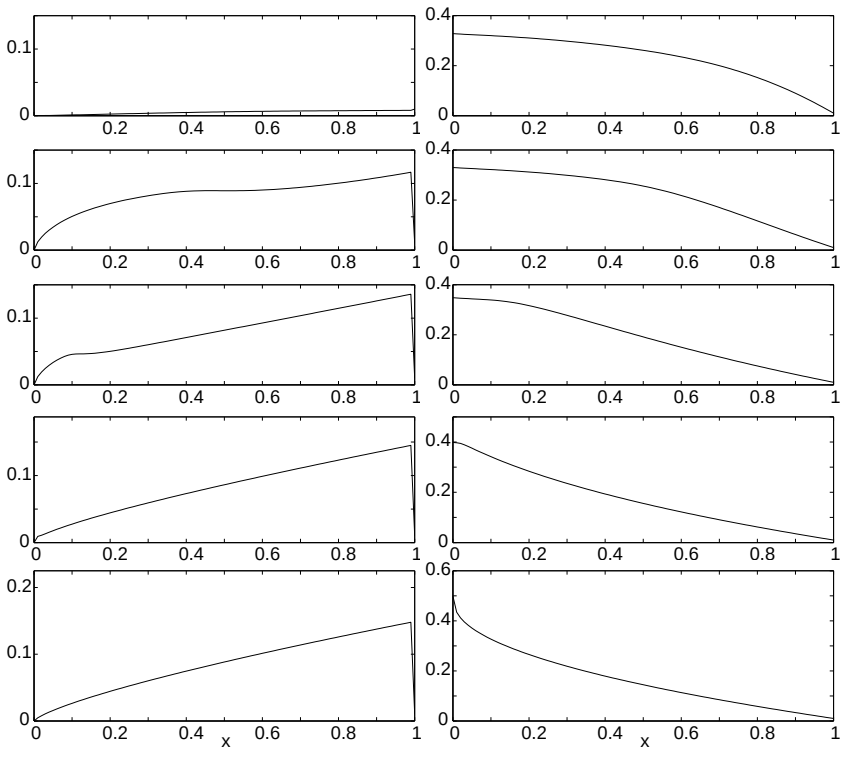

Figure 15: $h(x,t)$ and $H(x,t)$ for $7500 \leq t \leq 16\,000$

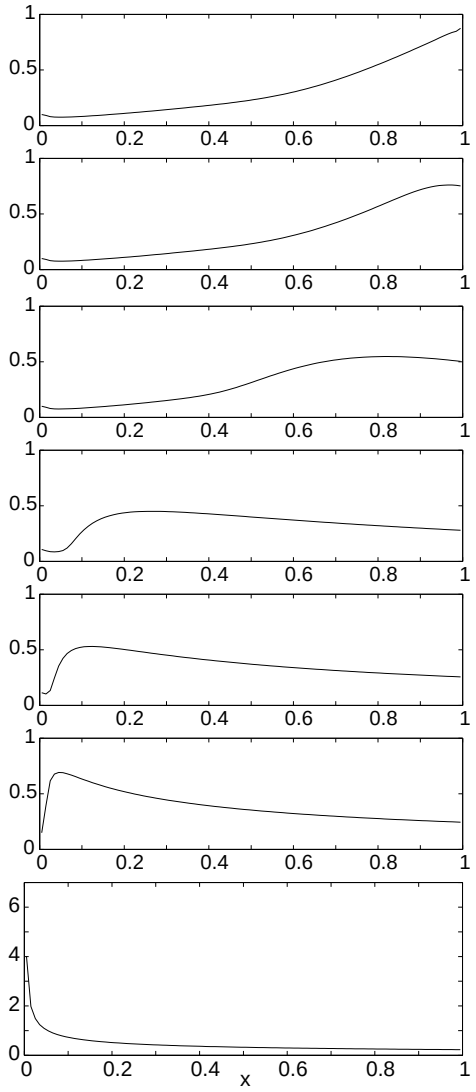

Figure 16: $S(x,t) = -H_x$ for $7500 \leq t \leq 16000$

switch to the single evolution of equations (23). The resulting slope profiles are graphed in Figure 16, where $t = 7500; 7510; 7600; 9\,000; 10\,000; 11\,000; 16\,000$.

The initial slope profile (at time 7500) is strictly increasing, corresponding to a convex water surface H; a maximum quickly forms on the right and travels across the domain until the slope $(-H_x)$ is strictly decreasing, giving a concave water surface.

The slope profile by time 11 000 may be only Hölder continuous, since it makes a rapid turn near $x = 0.05$. Thus the small initial concavity has been magnified into a shock: a knickpoint that travels upstream.

The final slope profile (at time 16 000) is graphed in Figure 17 against the predicted steady-state slope found by differentiating equation (24). Note that the predicted and observed slope profiles are nearly indistinguishable; the observed is slightly higher than the predicted.

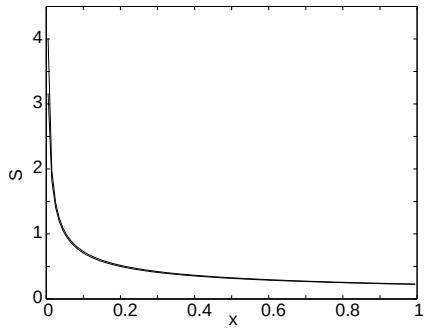

Figure 17: numerical $S(x, 16\,000)$ superimposed on $S_{ss}(x)$

6 Conclusion

The three shocks discussed in this paper tell a complete story. A small perturbation in the input of water gets magnified, forming a shock. The water depth shock makes a bore followed by a hydraulic jump. Together, these features create a young, convex hillslope. This hillslope is unstable; a small concavity at the bottom of the slope is magnified, forming a diffusive shock in the water surface slope that travels upslope and carves out a mature, concave landscape.

7 Acknowledgements

The authors would like to thank Terrence Smith for many helpful conversations. The first and the second authors were supported by grants number BCS-9819095, DMS-0072191 and DMS-0352563 from the National Science Foundation whose support is gratefully acknowledged. Some simulations were performed on a cluster of workstations, funded by a National Science Foundation SCREMS grant number DMS-0112388. The first and the third authors were supported by grant number DMS-

0244498 from the National Science Foundation, whose support is gratefully acknowledged, and grant number N000140410078 from the Offi ce of Naval Research, whose support is gratefully acknowledged.

References

[1] A. L. Bertozzi A. Munch. Rarefaction-undercompressive fronts in driven fi lms. *Physics of Fluids*, 11(10):2812–2814, 1999.

[2] Howard A.D. A detachment-limited model of drainage basin evolution. *Water Resources Research*, 30:2261–2285, 1994.

[3] B. Birnir, J. Hernández, and T. R. Smith. The stochastic theory of fluvial landsurfaces. *J. Nonlinear Science*, 2005. To appear.

[4] B. Birnir, T.R. Smith, and G. Merchant. The scaling of fluvial landscapes. *Computers and Geoscience*, 27:1189–1216, 2001.

[5] Loewenherz-Lawrence D.S. Stability and the initiation of channelized surface drainage: a reassessment of the short wavelength limit . *Journal of Geophysical Research*, 96:8453–8464, 1991.

[6] Loewenherz-Lawrence D.S. Hydrodynamic description for advective sediment transport processes and rill initiation. *Water Resources Research*, 30:3203–3212, 1994.

[7] H. P. Greenspan and R. E. Young. Flow over a containment dyke. *Proc. Roy. Soc. London. Series A*, 87:179–192, 1984.

[8] H. Huppert. Flow and instability of a viscous current down a slope. *Nature*, 300:427–429, 1982.

[9] Peter D. Lax. *Hyperbolic systems of conservation laws and mathematical theory of shock waves*. SIAM, 1973.

[10] R. J. LeVeque. *Numerical Methods for Conservation Laws*. Birkhauser-Verlag, Basel, 1990.

[11] G. E. Merchant. An elementary theory of drainage basin evolution. University of California, Santa Barbara, Department of Geography, Ph.D thesis, 2000.

[12] K. Mertens, V. Putkaradze, and P. Vorobieff. Braiding patterns on an inclined plane. *Nature*, 430:165, 2004.

[13] D. J. Needham and J. H. Merkin. On roll waves down an open inclined channel. *Proc. Roy. Soc. London. Series A*, 394:259–278, 1984.

[14] Horton R.E. Erosional development of streams and their drainage basins: a hydrophysical approach to quantitative morphology . *Geol. Soc. Am. Bull.*, 56:275–370, 1945.

[15] Kramer S. and M. Marder. Evolution of river networks. *Physical Review Letters*, 68:205–208, 1992.

[16] T.R. Smith, G.E. Merchant, and B. Birnir. Transient attractors: towards a theory of the graded stream for alluvial and bedrock channels. *Computers and Geosciences*, 26(5):531–541, 2000.

[17] E. F. Toro. Riemann problems and the waf method for solving the two-dimensional shallow water equations. *Phil. Trans. R. Soc. Lond. A*, 338:43–68, 1992.

[18] Smith T.R., B. Birnir, and G.E. Merchant. Towards an elementary theory of drainage basin evolution: I. the theoretical basis. *Computers and Geoscience*, 23(8):811–822, 1997.

[19] Smith T.R. and F.P. Bretherton. Stability and the conservation of mass in drainage-basin evolution . *Water Resources Research*, 8:1506–1529, 1972.

[20] Smith T.R., G.E. Merchant, and B. Birnir. Towards an elementary theory of drainage basin evolution: Iı. a computational evaluation. *Computers and Geoscience*, 23(8):823–849, 1997.

[21] E. W. Welsh. Landscape erosion: Convergence, singularities and shocks in a continous transport-limited model. Duke University, Department of Mathematics, Ph.D thesis, 2003.